Nuclear Engineering and Technology 56 (2024) 2842–2849

Contents lists available at ScienceDirect

Nuclear Engineering and Technology

journal homepage: www.elsevier.com/locate/net

Original Article

Characterization of glasses composed of PbO, ZnO, MgO, and B_2O_3 in terms of their structural, optical, and gamma ray shielding properties

Aljawhara H. Almuqrin [a], M.I. Sayyed [b,c,**], Ashok Kumar [d,e,*], U. Rilwan [f]

[a] Department of Physics, College of Science, Princess Nourah bint Abdulrahman University, P.O. Box 84428, Riyadh, 11671, Saudi Arabia
[b] Department of Physics, Faculty of Science, Isra University, Amman, Jordan
[c] Renewable Energy and Environmental Technology Center, University of Tabuk, Tabuk, 47913, Saudi Arabia
[d] University College, Benra, Dhuri, 148024, Punjab, India
[e] Department of Physics, Punjabi University, Patiala, 147002, Punjab, India
[f] Department of Physics, Faculty of Natural and Applied Sciences, Nigerian Army University, PMB 1500, Biu, Borno State, Nigeria

A R T I C L E I N F O

Keywords:
Radiation shielding
Band gap energy
Melt quenching technique
DASF
FTIR

A B S T R A C T

The amorphous glasses containing PbO, ZnO, MgO, and B_2O_3 have been fabricated using the melt quenching technique. The structural properties have been analysed using the Fourier-transform infrared (FTIR) and Raman spectroscopy. Derivative of Absorption Spectra Fitting (DASF) method have been used to estimate the band gap energy from the UV–Vis absorption data which decreases from 3.02 eV to 2.66 eV with increasing the concentration of the PbO.The four glass samples 0.284 and 0.826 MeV showed unique variations in terms of gamma attenuation ability. LZMB4 glass sample proved to be the mist effective in terms of shielding of gamma radiation as it requires little distance compared to LZMB3, LZMB2 and LZMB1 to attenuate. RPE revealed a raise with increase in the thickness of the material and reduces as the energy raises. TF is superior in LZMB1 compared to LZMB2, LZMB3 and LZMB4, confirming that, LZMB4 will attenuate better. The Z_{Eff} of the materials was seen falling as the energy increases, confirming that the linear attenuation coefficient of the glass materials decreases when the energy is increased. The results confirmed that, glass material LZMB4 is the best option especially for gamma radiation shielding applications compared to LZMB3, followed by LZMB2, then LZMB1.

1. Introduction

It is most necessary to impose radiation shielding protocols in order to stop the adverse health implications ionizing radiation on the sensitive equipment and well-being of human because of the threat it posed in different sectors [1]. This necessity was based on the fact that this radiation is highly ionizing, especially the gamma radiation with their ability to cause ionization in atoms, and subsequent disruption of the structures of molecules in a living tissue [2]. Sicknesses related to radiation, mutations in the cellular and damages in tissues are part of the serious health effects that might results from such ionization processes [3]. In places like hospitals where radiation is mostly employed in processes like imaging (diagnoses) and treatments (therapy), there is always an urgent need for shielding of such ionizing radiation [4]. This shielding urgency is based on the fact that the patients, the public and the health personnel needs to be protected against unwanted exposure to this harmful radiation while ensuring its benefits in medical procedures [5]. Being radiation a byproduct in nuclear power plants, it is similarly necessary to protect the workers as well as to prevent contamination of environment from this byproduct by employing as a matter of urgency, a strict shielding modality [6]. It is also important and necessary for industries with research laboratories, space explorations and non-destructive testing to shield their workers and their environments from these challenges of radiation exposure [7]. More so, since there is advancement in the technological applications of ionizing radiation, it is also a requirement to shield electronic components in order to prevent them from damaging and also to be sure of the sensitive instrument's integrity [8]. Accordingly, different materials such as ceramics, alloys, glasses and others are used for radiation shielding purpose.

Structural assessment of glass entails complex analysis of the glass's compositions, crystalline structures and density, as such features notably improve the gamma radiation attenuating ability [9]. Since

* Corresponding author. University College, Benra, Dhuri, 148024, Punjab, India.
** Corresponding author. Department of Physics, Faculty of Science, Isra University, Amman, Jordan.
E-mail addresses: dr.mabualssayed@gmail.com (M.I. Sayyed), ajindal9999@gmail.com (A. Kumar).

https://doi.org/10.1016/j.net.2024.02.047
Received 17 January 2024; Received in revised form 20 February 2024; Accepted 24 February 2024
Available online 26 February 2024

different glasses responds to radiation differently, it is necessary to have clear apprehension in order to have direction while fabricating these glasses for a particular purpose [10].

The crystal structure and the density of a glass material have advance impact on the glass's attenuation ability, promising that the choice of the glass material gives an improved fencing in opposition to radiation [11]. At the same time, optical features such as lucidity, dispersive nature and index of refraction plays an important part in practical applications of such glasses [12].

In places like nuclear power plants as well as medical tools where there is need to be monitoring and seeing the procedures going on, optically transparent materials for shielding are most needed [13]. There is hence need for a detailed study on the optical and structural features of glasses to be applied for shielding purposes in order to delicately maintain efficiency in protection against radiation and practical utilization, putting the glass in order with the demand of different industries [14].

Despite the advantages of glasses in shielding applications, glasses comprising of PbO, ZnO, MgO and B_2O_3 might have more advantage in terms of shielding applications over other glasses [15]. This may be due to their high optical and structural properties. PbO play an important part in shielding gamma radiation effectively because of its high Z [16]. Introduction of MgO and ZnO also may increase the quality of the structure while retaining the lucidity (an important prerequisite in a purpose where transparency is required) [17,18]. B_2O_3 serve to customize the glass matrix to an appreciable level, determining features like heat expansion and density [19]. Mutual exchange between PbO, ZnO, MgO and B_2O_3 produces glass materials which succeeds both optically and structurally [20]. Such glass materials provide a lucent fence, solving the double disputes of giving structural equilibrium and effective shielding of gamma radiation [21]. Also, comparing these glass materials with other conventional materials such as concrete or lead, these glass compositions give a diverse solution, promising efficient protection against gamma radiation with no compromise to visible features of the glasses [22]. This edge is especially vital in health or medical settings, making it possible for procedures like diagnoses where regular observation is required [23]. The proceeding significance on analyzing and upgrading such glass materials implies a tactical method of improving materials for shielding against radiation, offering solutions which does not only solve the present disputes but equally clear ways for later technologies in protection against ionizing radiation [24].

We have studied the physical and mechanical properties of the PbO–ZnO–MgO–B_2O_3 glasses in our previous reporting [25]. In continuation of this research work, we characterized glasses composing of PbO, ZnO, MgO, and B_2O_3 in terms of their structural, optical, and gamma ray shielding properties for ionizing radiation shielding applications.

2. Materials and methods

2.1. Preparation of samples

The fabrication of PbO–ZnO–MgO–B_2O_3 glasses involved the use of the melt-quenching technique. In the initial phase, oxides of the AR grade of desired quantity as specified in Table 1 were weighed using an electronic scale with a precision of 0.001 g. Creating a reliable blend with the use of an agate mortar, essential for breaking down an array of chemicals into fine particles. The resultant mixture was carefully placed in an alumina crucible within a muffle furnace. The furnace was heated to 1050 °C and maintained at this temperature for 2 h, with periodically stirring the molten mixture to ensure even distribution of the components. Subsequently, another furnace with graphite mold was kept at 300 °C during the annealing process. The molten material was poured into the graphite mold. The purpose of the annealing process was to mitigate internal stress in the material, thus minimizing the risk of breakage. The densities of the prepared glasses have been measured using the Archimedes' principle as described in our previous reporting [25].

Table 1
Composition and Optical parameters.

Sample code	Moles of oxides present				ρ (g/cm^3)	E_g (eV)
	PbO	ZnO	MgO	B_2O_3		
LZMB1	0.45	0.1	0.1	0.35	4.701	3.02
LZMB2	0.5	0.1	0.1	0.3	5.044	2.91
LZMB3	0.55	0.1	0.1	0.25	5.366	2.81
LZMB4	0.6	0.1	0.1	0.2	5.687	2.66

2.2. X-ray diffraction (XRD) spectroscopy

X-ray diffraction analysis is conducted using the Panalytical X'Pert Pro X-Ray Diffractometer. The instrument utilizes Cu-K_α radiations with a wavelength of 1.54 Å, operating at 45 kV and 40 mA, covering a 2θ range from 2^o to 90^o.

2.3. FTIR spectroscopy

Perkin Elmer-2, an advanced FTIR apparatus, was used to capture the FTIR spectra spanning a broad wavelength from 4000 to 400 cm^{-1} using KBr as a matrix.

2.4. Raman spectroscopy

The high-resolution STR500Airix Confocal Raman Spectrometer with PL with precision levels below 0.5 cm^{-1} was used to record the Raman spectra. This system utilizes a 532 nm laser.

2.5. UV–Vis spectroscopy

By analysing its UV–Vis absorption data, the DASF approach may be employed to ascertain the energy band gap (E_g) of a substance [26–28]. The DASF method provides a systematic approach for extracting information about the energy band gap from UV–Vis absorption data without requiring detailed knowledge about the specific nature of electronic transitions. It leverages the discontinuity in the derivative plot to pinpoint the wavelength associated with the band gap, allowing for the determination of the material's optical band gap energy. The DASF method involves the analysis of the derivative of a particular expression related to the absorption data. The expression is given by Refs. [27,28]:

$$\frac{d\left\{ln\left[\frac{A(\lambda)}{\lambda}\right]\right\}}{d\left\{\frac{1}{\lambda}\right\}}=\frac{m}{\left(\frac{1}{\lambda}-\frac{1}{\lambda_g}\right)} \tag{1}$$

Where A(λ) is the absorption intensity at a given wavelength λ, m is a constant and λ_g is the wavelength at which the derivative plot has a discontinuity.

2.6. Phy-X/PSD software

For the theoretical assessment of a material's radiation shielding effectiveness, the Phy-X/PSD software is used [29]. It is a online simulation tool that requires the material's densities and chemical compositions as input and provides a specific set of shielding parameters at required energies as an output.

3. Results and discussion

3.1. Structural analysis

The obtained XRD spectra for the studied materials are shown in Fig. 1. The lack of a sharp peak and the presence of two wide humps between 20° and 37° and 40° and 60° respectively demonstrate that the structures of glasses are amorphous [30,31]. The d-spacing variations within the glass network are responsible for the formation of broad humps in the spectra.

Fig. 2 presents the FTIR spectra in the 400-1800 cm^{-1} range of the LZMB glass series. It can be divided into four significant regions. In Region-I, spanning 400-550 cm^{-1}, we observe small peaks about ~450 cm^{-1} and ~500 cm^{-1}, which are associated with the vibrations of O–Pb^{2+}, O–Zn^{2+}, and O– Mg^{2+} [32,33] which becomes prominent with the increasing concentration of PbO as network modifier PbO fills empty spaces between [BO_3] units with Pb^{2+} ions [34]. An increase in PbO content affects the electrostatic fields of the highly polarizing Pb^{2+} ions, potentially leading to an increase in the wavenumber of B–O–B bending vibrations [35]. Region II, spanning 550–770 cm^{-1}, correlates with the B–O–B bending modes of BO_3 units [36]. The absorption about ~620 cm^{-1} may corresponds to the bending of O–B–O bonds or to the vibration of PbO [34,36]. Lead plays a dual function. When these cations create ionic bonds, it functions as a network modifier. Secondly, it act as glass formers when Pb–O is covalent [37]. Thus lead ions have the potential to create BO_4 tetrahedra by disturbing the network. The bending of B–O–B correlations extends to 707 cm^{-1} [38,39]. Region-III, stretching from 770 to 1100 cm^{-1}, corresponds to the stretching of B–O bonds in (BO_4) units [40]. The vibrations in this region can be due to stretching vibrations of B–O and stretching vibrations of BO_4 tetrahedra about ~815 cm^{-1}, ~905 cm^{-1}, and ~995 cm^{-1} [41]. Region-IV, spanning 1100-1500 cm^{-1}, involves B–O stretching in BO_3 and BO_2O^- units [42]. In contrast to the second zone, the last FTIR region, which extends from 1100 to 1500 cm^{-1}, shows more pronounced bands, which represent the stretching vibrations of the trigonal BO_3 structural units. Within the $(BO_3)^{3-}$ unit, the stretching vibrations of the B–O bonds are reflected by the band at around 1250 cm^{-1}. The majority of this process relies on oxygen atoms bonding with various groups [43,44]. B–O asymmetric stretching causes the band about 1290 cm^{-1} [45]. At about 1383 cm^{-1}, metaborates, pyroborates, and orthoborates experience the stretching vibrations of B–O trigonal $(BO_3)^{3-}$ groups [46].

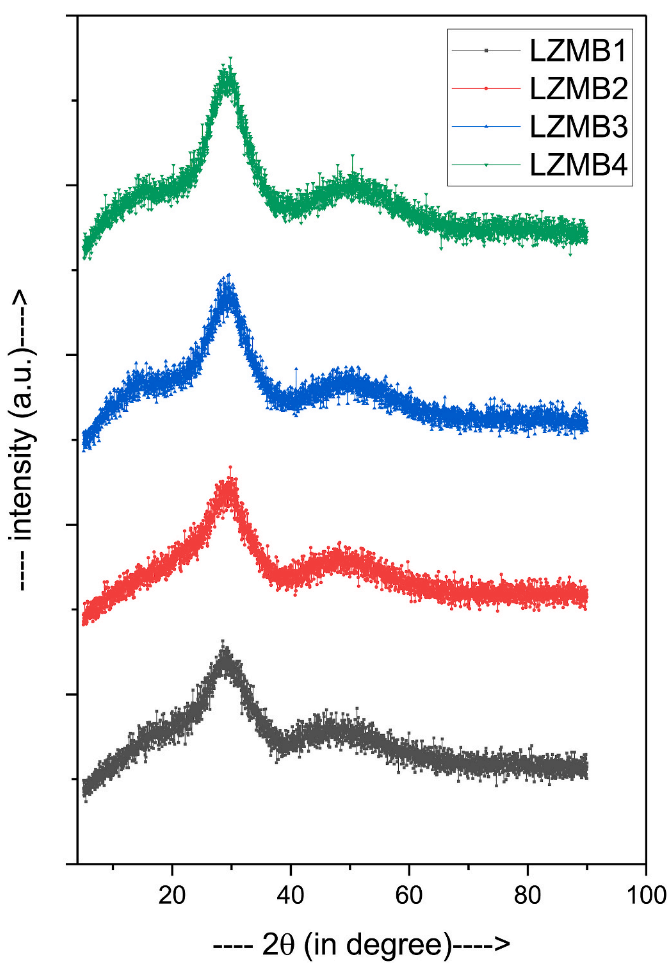

Fig. 1. XRD plot for different samples.

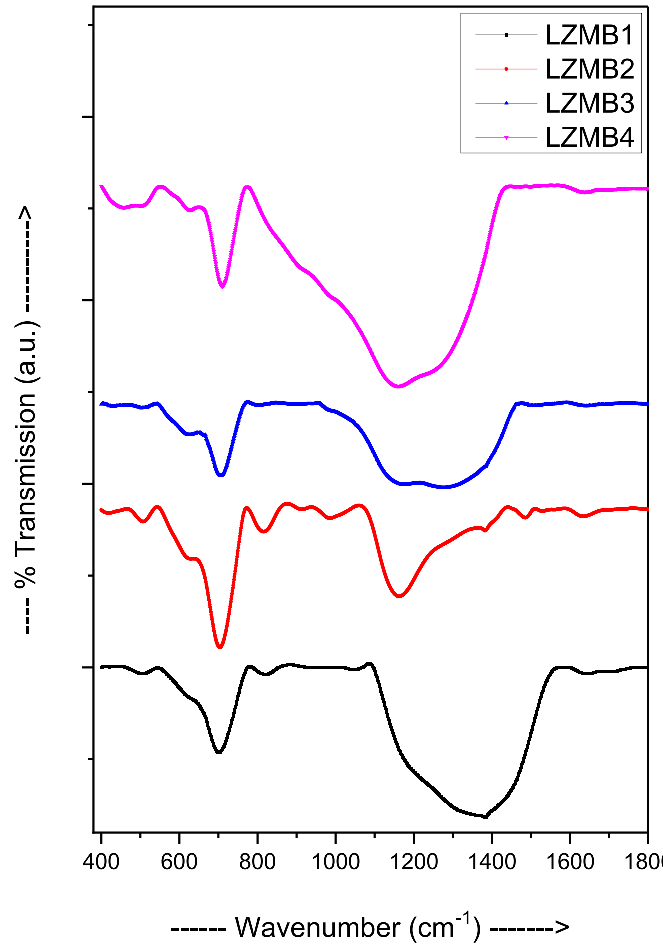

Fig. 2. FTIR plot for different samples.

The Raman spectra of the glasses under investigation (Fig. 3) display peaks within the range of 100–1600 cm^{-1}. The Raman spectra have revealed the presence of eight prominent peaks about 144, 292, 622, 725, 930, 999, 1250, and 1284 cm^{-1}. The presence of a peak about 144 cm^{-1} might be attributed to the structural arrangement of the PbO_4 pyramid, where Pb^{2+} ions coordinate with the pyramid's apex four times [47,48]. The highly polarised shoulder, which occurs at around 292 cm^{-1}, is attributed to the bending modes of ZnO_4 units [49]. The band seen about 622 cm^{-1} was assigned to the bending mode of the Pb–O–B links and the localised breathing movements of oxygen atoms in the boroxol ring [50,51]. The strength of the band about 725 cm^{-1}, formed due to the presence of metaborate groups, decreases with PbO content. The formation of orthoborate and pyroborate groups are responsible for the Raman bands about 930 cm^{-1} and 1250 cm^{-1} respectively [52]. The kink observed about 919 cm^{-1} in LZMB3 and LZMB4 samples corresponds to the elongation vibrations of B–O bonds in orthoborate

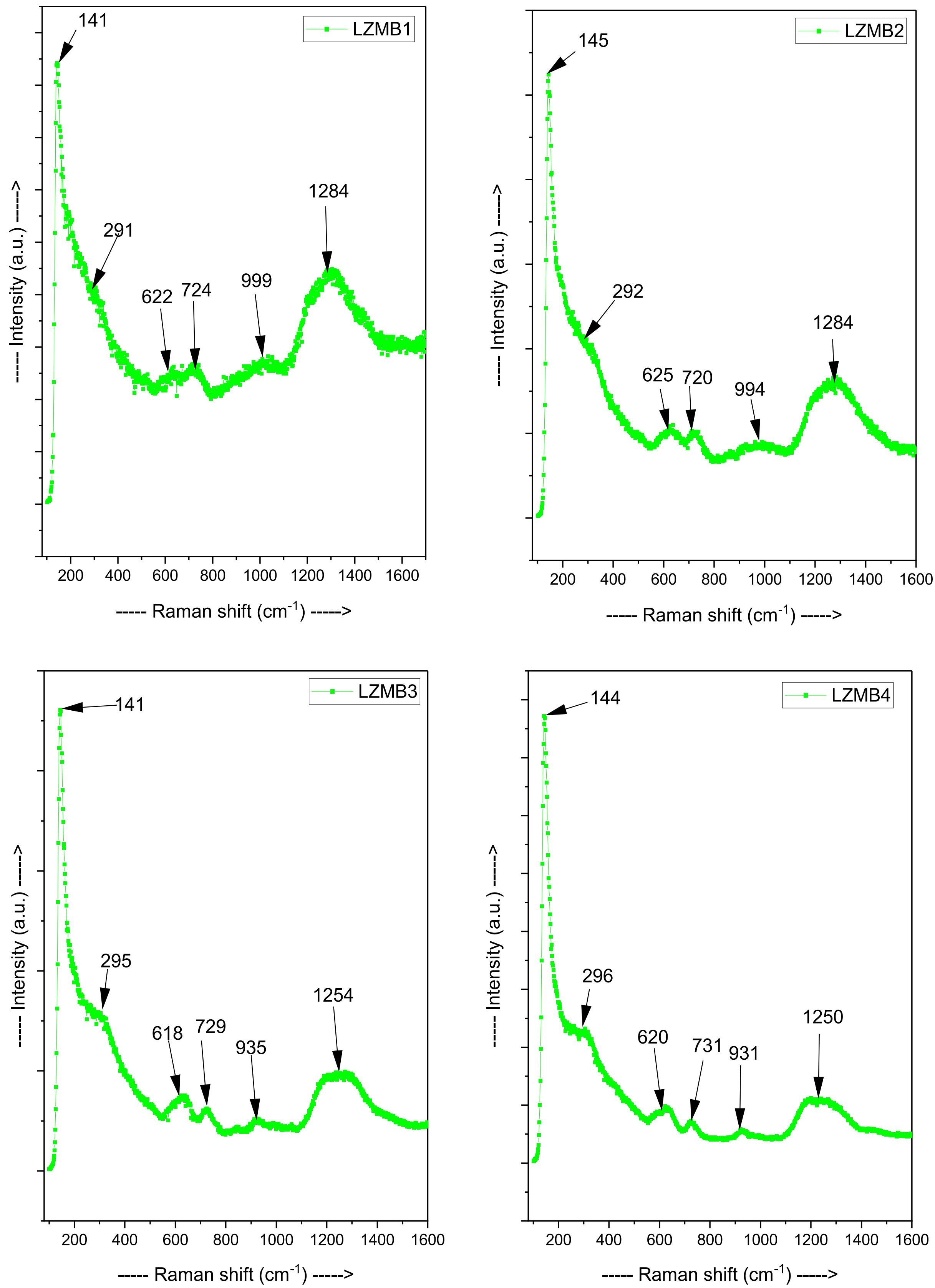

Fig. 3. Raman plot for different samples.

structures composed of pyramidal BO_3 units [53]. The wide spectral range centred about 930 cm^{-1} may be attributable to the asymmetric stretching motion of anions in B–O–Pb, B–O–Bi, and/or B–O–Zn bridges. The peak about ~919 cm^{-1} is missing in LZMB1 and LZMB2 samples where another peak around ~999 cm^{-1} represents the B–O stretching vibration of tetrahedral BO_4 in BO_3 orthoborate units [54]. The band at 1284 cm^{-1} is the cause of B –O– vibrations in ortho and pyroborate segments [40,54].

3.2. Optical analysis

Then $\frac{d\{ln|\frac{A(\lambda)}{\lambda}|\}}{d\{\frac{1}{\lambda}\}}$ is plotted against $\frac{1}{\lambda}$ in Fig. 4. The discontinuity in the plot signifies a unique point where the derivative experiences a sudden change. This point is $\frac{1}{\lambda} = \frac{1}{\lambda_g}$, and it represents the wavelength at which the material undergoes an electronic transition. The wavelength λ_g corresponding to the discontinuity is then used to determine E_g using the relationship:

$$E_g = \frac{1239.82}{\lambda_g} eV \tag{2}$$

From Fig. 4, the discontinuity corresponding to $\frac{1}{\lambda} = \frac{1}{\lambda_g}$ are 0.002436 nm^{-1}, 0.002349 nm^{-1}, 0.002266 nm^{-1} and 0.002147 nm^{-1} respectively for the LZMB1, LZMB2, LZMB3 and LZMB4 samples. From the reciprocal of these values, one can find the value of λ_g which is equal to 410.51 nm, 425.71 nm, 441.31 nm and 465.77 nm respectively for the LZMB1, LZMB2, LZMB3 and LZMB4 samples. Using the expression from Eq. (2), one can find the E_g which is equal to 3.02eV, 2.91 eV, 2.81 eV and 2.66 eV respective for the LZMB1, LZMB2, LZMB3 and LZMB4 samples. It suggests that the amount of energy necessary for electronic transitions inside the glass structure has also reduced. This is because of the structural alterations that are caused due to weakening of the metal oxygen bond which results is an increase in the number of non-bridging oxygens (NBOs) [55]. Thus inclusion of PbO promotes the creation of NBOs in the glass matrix, which provide new energy levels to the band structure and, as a result, reduce the energy required to bridge the band gap.

3.3. Gamma ray shielding analysis

Fig. 5 presented the analysis of the HVL, TVL and MFP each at energy of 0.284 MeV. It could be observed in Fig. 5 that, for glass sample LZMB1, the distance required to reduce the energy of 0.284 MeV to half (0.142 MeV) is 0.429 cm while glass sample LZMB2, LZMB3 and LZMB4 at the same energy, required 0.386 cm, 0.352 cm and 0.323 cm respectively to achieve the same goal. It obviously be seen from the same Figure that, in glass sample LZMB1, the distance needed to attenuate the energy of 0.284 MeV to tenth (0.0.0284 MeV) is 1.425 cm while glass sample LZMB2, LZMB3 and LZMB4 at the same energy, required 1.282 cm, 1.169 cm and 1.073 cm respectively to achieve the same aim.

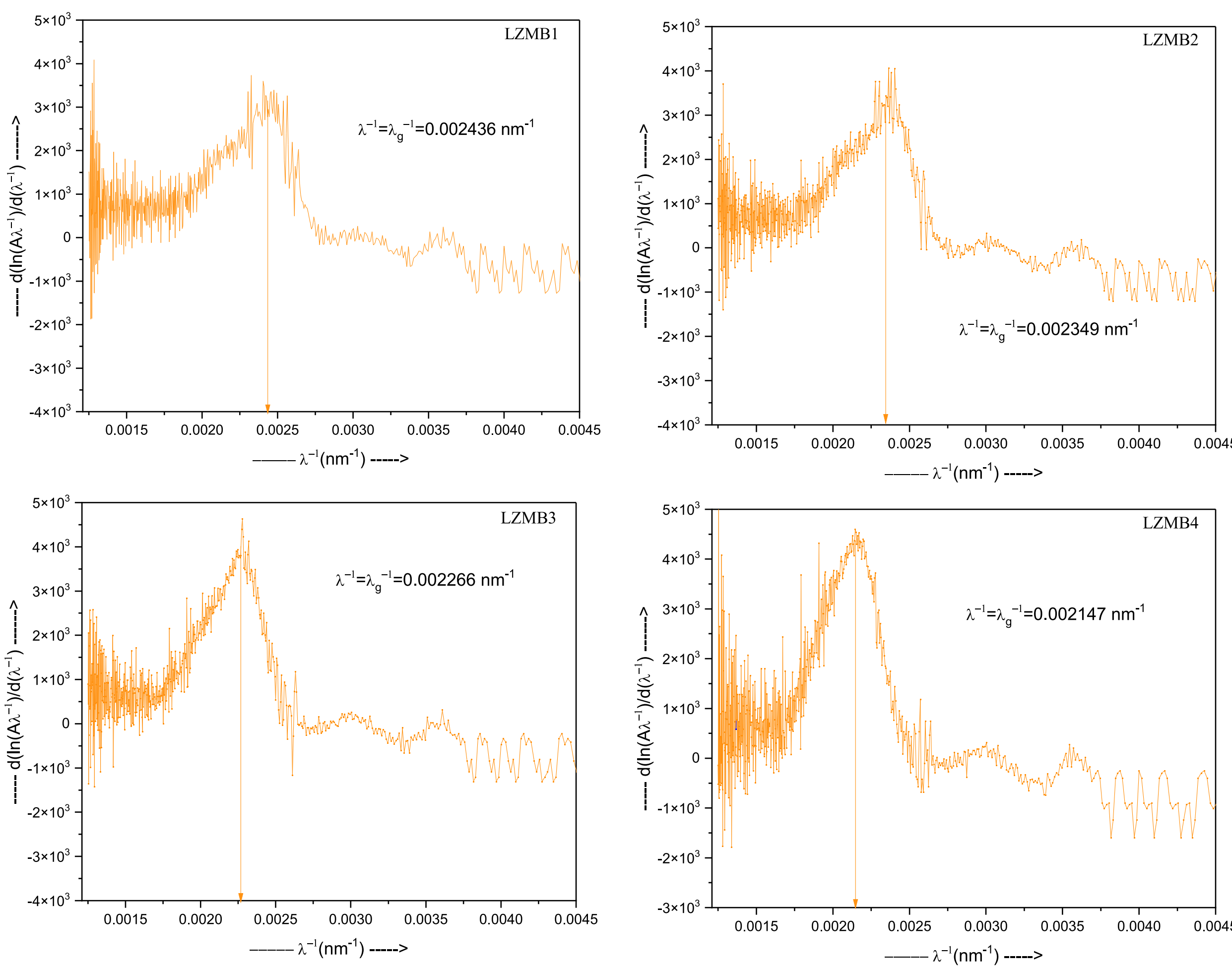

Fig. 4. $\frac{d\{ln|\frac{A(\lambda)}{\lambda}|\}}{d\{\frac{1}{\lambda}\}}$ vs. $\frac{1}{\lambda}$ plot for different samples.

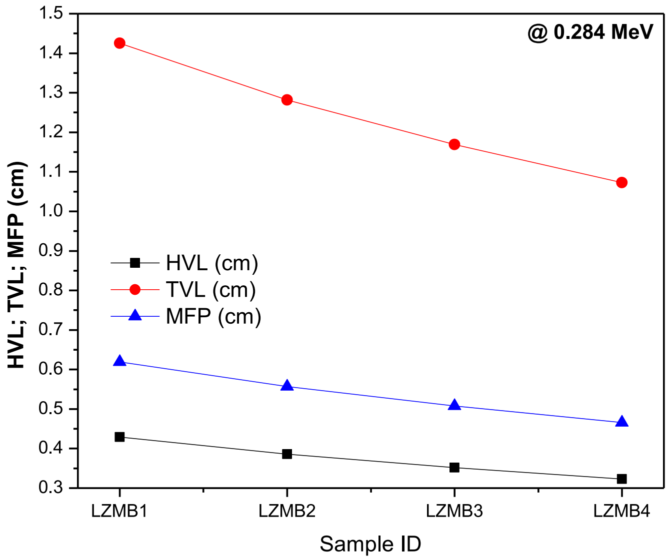

Fig. 5. HVL, TVL, MFP Plots for different samples at 0.284 MeV.

Moreover, it is clearly seen that, in glass sample LZMB1, the distance that must be needed to for possible interaction is 0.619 cm while glass sample LZMB2, LZMB3 and LZMB4 at the same energy, required 0.557 cm, 0.508 cm and 0.466 cm respectively to achieve the same aim.

Fig. 6 presented the analysis of the HVL, TVL and MFP each at energy of 0.826 MeV. A similar trend to that of Fig. 5 could be observed in Fig. 6, with glass sample LZMB1 requiring a distance of 1.84 cm to attenuate 0.826 MeV photons by 90%, while glass sample LZMB2, LZMB3 and LZMB4 at the same energy, will need 1.701 cm, 1.588 cm and 1.489 cm respectively to achieve 90% attenuation. It is also clear from Fig. 6 that, glass sample LZMB1 required a distance of 6.112 cm to attenuate 0.826 MeV photons to tenth of its initial intensity, while glass samples LZMB2, LZMB3 and LZMB4 at the same energy, needs 5.652 cm, 5.276 cm and 4.947 respectively to achieve the same attention. From same Figure, it is clearly seen that, in glass sample LZMB1, the distance that must be needed to for possible interaction is 2.655 cm while glass samples LZMB2, LZMB3 and LZMB4 at the same energy, required 2.455 cm, 2.291 cm and 2.148 cm respectively to similarly have one possible interaction each. The result implied that, less distance is required for photon energy in the material LZMB4 to get attenuated compared to LZMB3, then LZMB2 and LZMB1 with the highest required distance, making LZMB4 the better material in terms of gamma radiation shielding applications compared to other examined materials.

Also, RPE of LZMB1 has been computed at different thickness and presented in Fig. 7. Based on Figure, it is clear that the radiation shielding efficiency (RPE) increased with enhanced thickness of the material, and also falls with raise in energy. This could be observed from the chart (Fig. 7), since at x = 1.2 cm, the material exhibits better RPE when compared RPE at x = 0.75 cm, and when x = 0.5 cm the material exhibits the lowest RPE.

Raise in radiation transmission factor (TF) leads to fall in linear attenuation coefficient (μ), as TF is a reciprocal of μ. Fig. 8 present the computed results for TF of all samples at thickness of x = 0.5 cm. It could be seen that, at varying energies, the TF was highest in glass sample LZMB1, followed by glass sample LZMB2, then glass sample LZMB3 and glass sample LZMB4 has the lowest TF. This confirmed that the glass material LZMB4 has better attenuation, followed by LZMB3, then LZMB2 with LZMB1 having the lowest radiation attenuation.

In Fig. 9, the HVL for the prepared glasses have been compared to other glasses [56]. Clearly, the HVL for LZMB1 is lower than $14PbO–21PbF_2–35B_2O_3–30SiO_2$, while the HVL for LZMB2 is lower than $14PbO–28PbF_2–28B_2O_3–30SiO_2$ and LZMB4 glass has lower HVL than all the $PbO–PbF_2–B_2O_3–SiO_2$ glasses.

4. Conclusion

The $PbO–ZnO–MgO–B_2O_3$glasseshave been fabricated using the melt quenching technique. The XRD spectroscopy reveals that glasses are amorphous. The various kinds of the stretching and bending modes vibration and the presence of different structural units have been revealed using FTIR and Raman spectroscopy. The DASF method have been used to estimate the E_g from the UV–Vis absorption data. The $E_g$decreases from 3.02 eV to 2.66 eV with increasing the concentration of the PbO. The four glass samples 0.284 and 0.826 MeV showed unique variations in terms of gamma attenuation ability. LZMB4 glass sample proved to be the mist effective in terms of shielding of gamma radiation as it requires little distance compared to LZMB3, LZMB2 and LZMB1 to attenuate. RPE revealed a raise with increase in the thickness of the material and reduces as the energy raises. TF is superior in LZMB1 compared to LZMB2, LZMB3 and LZMB4, confirming that, LZMB4 will attenuate better. The HVL results showed that LZMB1 requiring a distance of 1.84 cm to attenuate the energy of 0.826 MeV by 90%, while glass sample LZMB2,

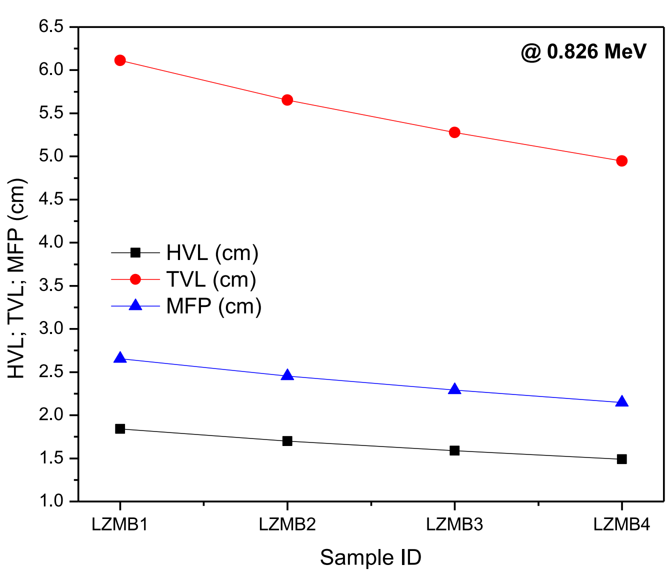

Fig. 6. HVL, TVL, MFP Plots for different samples at 0.826 MeV.

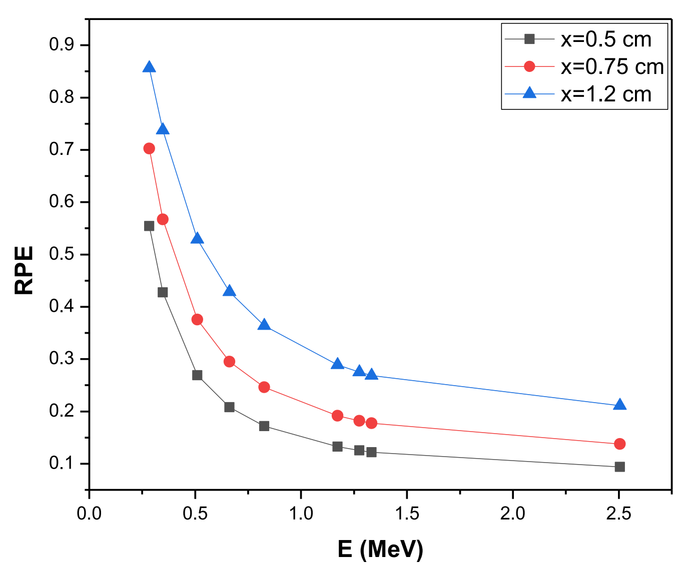

Fig. 7. RPE Plots for different samples versus energy at some selected thicknesses.

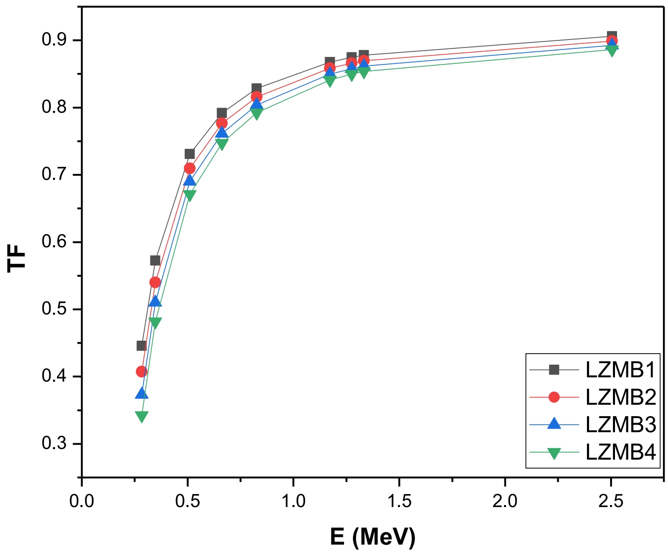

Fig. 8. TF Plots for different samples versus energy.

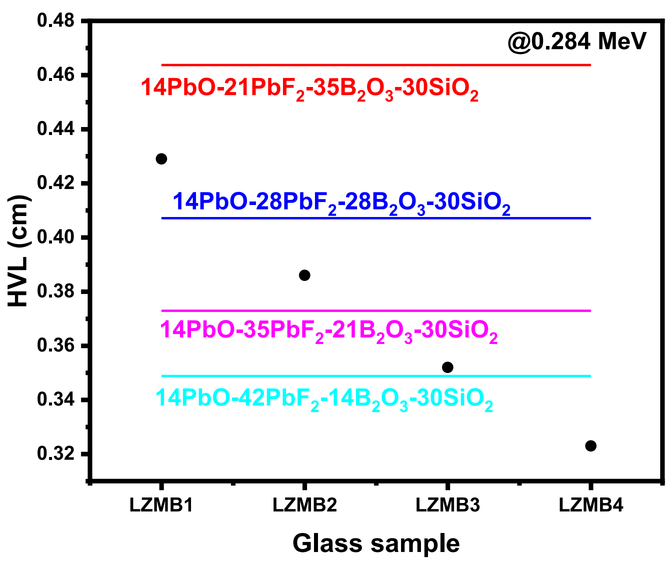

Fig. 9. Comparison of the HVL of the present glasses with $PbO–PbF_2–B_2O_3–SiO_2$ glasses.

LZMB3 and LZMB4 at the same energy, will need 1.701 cm, 1.588 cm and 1.489 cm respectively to achieve 90% attenuation.

Declaration of competing interest

The authors declare that they have no known competing financial interests or personal relationships that could have appeared to influence the work reported in this paper.

Acknowledgment

The authors express their gratitude to the Princess Nourah bint Abdulrahman University Researchers, Supporting Project Number (PNURSP2024R2), Princess Nourah bint Abdulrahman University, Riyadh, Saudi Arabia.

References

[1] Hanan Al-Ghamdi, Ashok Kumar, J.F.M. Jecong, Aljawhara H. Almuqrin, D. I. Tishkevich, M.I. Sayyed, Optical and gamma ray shielding behavior of PbO-B2O3-CuO-CaO Glasses, J. Mater. Res. Technol. 18 (2022) 2494–2505, https://doi.org/10.1016/j.jmrt.2022.03.120.

[2] S.M. Tajudin, A.H.A. Sabri, M.Z. Abdul Aziz, S.F. Olukotun, B.M. Ojo, M.K. Fasasi, Feasibility of clay-shielding material for low-energy photons (gamma/X), Nucl. Eng. Technol. 51 (2019) 1333–1337, https://doi.org/10.1016/j.net.2019.04.020 (South Korea).

[3] M.Y. Hanfi, M.I. Sayyed, E. Lacomme, I. Akkurt, K.A. Mahmoud, The influence of MgO on the radiation protection and mechanical properties of tellurite glasses, Nucl. Eng. Technol. 53 (2021) 2000–2010, https://doi.org/10.1016/j.net.2020.12.012.

[4] Vijay L. Gurav, Rajesh A. Samant, Satish B. Manjare, Urmila K. Patil, Sana R. Solkar, Shivani S. Moghe, Biosynthesis of calcium oxide nanoparticles using Ocimum sanctum (Tulsi) leaf extracts and screening its antimicrobial activity, Asian Journal of Nanoscience and Materials 3 (2) (2020) 115–120, 26655./AJNANOMAT.2020.2.3.

[5] S.F. Olukotun, S.T. Gbenu, O.F. Oladejo, F.O. Balogun, M.I. Sayyed, S.M. Tajudin, E.I. Obiajunwa, M.K. Fasasi, The effect of incorporated recycled low-density polyethylene (LDPE) on the fast neutron shielding behaviour (FNSB) of clay matrix using MCNP and PHITS Monte Carlo codes, Journal of Radiation Physics and Chemistry 182 (2021) 109351–109357, https://doi.org/10.1016/j.radphyschem.2021.109351(UnitedKingdom.

[6] A. Aşkın, M.I. Sayyed, Amandeep Sharma, M. Dal, R. El-Mallawany, M.R. Kaçal, Investigation ofthe gamma ray shielding parameters of (100-x) [0.5Li2O–0.1B2O3–0.4P2O5]-xTeO2 glasses using Geant4 and FLUKA codes, J. Non Cryst. Solids 521 (2019) 119489, https://doi.org/10.1016/j.jnoncrysol.2019.119489.

[7] A.H. Aminordin Sabri, M.Z. Abdul Aziz, S.F. Olukotun, F. Tabbakh, S.M. Tajudin, Study on the shielding materials for low-energy gamma sources, IOP Conf. Ser. Mater. Sci. Eng. 785 (2020) (2020) 012007, https://doi.org/10.1088/1757-899X/785/1/012007 (United Kingdom).

[8] M.I. Sayyed, Hakan Akyildirim, M.S. Al-Buriahi, Eloic Lacomme, Rachid Ayad, Giovanni Bonvicini, Oxyfluoro-tellurite-zinc glasses and the nuclear-shielding ability under the substitution of AlF_3 by ZnO, Appl. Phys. A. 126 (2020) 88, https://doi.org/10.1007/s00339-019-3265-6.

[9] M.I. Sayyed, G. Lakshminarayana, M.G. Dong, M.Ç. Ersundu, A.E. Ersundu, I. V. Kityk, Investigation on gamma and neutron radiation shielding parameters for BaO/SrO−Bi2O3−B2O3 glasses, Radiat. Phys. Chem. 145 (2018) 26–33, https://doi.org/10.1016/j.radphyschem.2017.12.010.

[10] S.F. Olukotun, K.S. Mann, S.T. Gbenu, F.I. Ibitoye, O.F. Oladejo, A. Joshi, H. O. Tekin, M.I. Sayyed, M.K. Fasasi, F.A. Balogun, T. Korkut, Neutron-shielding behaviour investigations of some clay-materials, Nucl. Eng. Technol. 51 (2019) 1444–1450, https://doi.org/10.1016/j.net.2019.03.019(SouthKorea.

[11] Qiuling Chen, K.A Naseer, K. Marimuthu, P. Suthanthira Kumar, Baoji Miao, K. A. Mahmoud, M.I. Sayyed, Influence of modifier oxide on the structural and radiation shielding features of Sm3+-doped calcium telluro-fluoroborate glass systems, J. Aust. Ceram. Soc. 57 (2021) 275–286, https://doi.org/10.1007/s41779-020-00531-8.

[12] S.F. Olukotun, M.I. Sayyed, O.F. Oladejo, N. Almousa, S.A. Adeojo, E.O. Ajoge, S. T. Gbenu, M.K. Fasasi, Computation of gamma buildup factors and heavy ions penetrating depths in clay composite materials using Phy-X/PSD, EXABCal and SRIM Codes, Coatings 12 (2022) (2022), https://doi.org/10.3390/coatings12101512 (Switzerland).

[13] M.G. Dong, O. Agar, H.O. Tekin, O. Kilicoglu, M. Kaky Kawa, M.I. Sayyed, A comparative study on gamma photon shielding features of various germanate glass systems, Composites, Part B 165 (2019) 636–647.

[14] Heba Jamal Alasali, M.I. Sayyed, Studies of gamma radiation attenuation properties of silica-based commercial glasses utilized in Jordanian dwellings, Opt. Quant. Electron. 56 (2024) 391, https://doi.org/10.1007/s11082-023-05941-z.

[15] Soheila Ghasemi, Fatemeh Badri, Hadieh Rahbar Kafshboran, Pd catalyst supported thermo-responsive modified poly(*N*-isopropylacrylamide) grafted Fe3O4@CQD@Si in heck coupling reaction, Asian Journal of Green Chemistry 8 (1) (2024) 39–56, https://doi.org/10.48309/ajgc.2024.408188.1401.

[16] Haytham A. Ayoub, Khairy Mohamed, Farouk A. Rashwan, Hanan F. Abdel-Hafez, Synthesis of calcium silicate hydrate from chicken eggshells and combined joint effect with nervous system insecticides, Asian Journal of Green Chemistry 6 (2) (2022) 103–111, https://doi.org/10.22034/ajgc.2022.2.1.

[17] Hurieh Mohammadzadeh, Roya Roohibakhsh, Hamid Reza Rezaie, An investigation on sintering behavior of nanostructured Cu-10, 20 wt. % Ni alloy powders, Asian Journal of Nanoscience and Materials 4 (2) (2021) 95–112, https://doi.org/10.26655/AJNANOMAT.2021.2.1.

[18] Fatemeh Banifatemeh, Polymerization of graphite and carbon compounds by aldol condensation as anti-corrosion coating, Asian Journal of Green Chemistry 7 (1) (2023) 25–38, https://doi.org/10.22034/ajgc.2023.1.4.

[19] Mohammad Reza Jalali Sarvestani, The effect of doping graphene with silicon on the adsorption of cadmium(II): theoretical investigations, Asian Journal of Nanoscience and Materials 3 (4) (2020) 280–290, https://doi.org/10.26655/AJNANOMAT.2020.4.2.

[20] Ashraf Heidaripour, Fateme Salmani, Study of PbS quantum dots (QDs) and proposing Pb@PbS-QD@CdSe for new generation of LEDs, Asian Journal of Green Chemistry 8 (1) (2024) 15–24, https://doi.org/10.48309/ajgc.2024.406146.1398.

[21] Yaghoub Ahmadyousefi, A brief overview of plant-derived chemotherapeutic agents for cancer therapy, Asian Journal of Green Chemistry 7 (3) (2023) 175–179, https://doi.org/10.22034/ajgc.2023.388922.1375.
[22] Yaghoub Ahmadyousefi, Bacteria-derived chemotherapeutic agents for cancer therapy: a brief overview, Asian Journal of Green Chemistry 7 (4) (2023) 223–228, https://doi.org/10.22034/ajgc.2023.388927.1376.
[23] Jude N. Udeh, Agnes C. Nkele, Raphael M. Obodo, Innocent C. Nwodo, Chinedu P. Chime, Assumpta C. Nwanya, Maaza Malik, Fabian I. Ezema, Investigating the properties of cobalt phosphate nanoparticles synthesized by co-precipitation method, Asian Journal of Nanoscience and Materials 5 (1) (2022) 22–35, https://doi.org/10.26655/AJNANOMAT.2022.1.3.
[24] Abolfazl Khodadadi, Mohammad Rahim Talebtash, Investigation and synthesis of Fe doped *Al2O3* nanoparticles by Co-precipitation and sol gel methods, Asian Journal of Nanoscience and Materials 5 (1) (2022) 36–47, https://doi.org/10.26655/AJNANOMAT.2022.1.4.
[25] Dalal A. Aloraini , Ashok Kumar, Aljawhara H. Almuqrin and Mohammad Ibrahim Abualsayed, An exploration of the physical, optical, mechanical, and radiation shielding properties of PbO–MgO–ZnO–B2O3 glasses, Open Chem., https://doi.org/10.1515/chem-2023-0104.
[26] Dariush Souri, Zahra Esmaeili Tahan, A new method for the determination of optical band gap and the nature of optical transitions in semiconductors, Appl. Phys. B 119 (2015) 273–279.
[27] B.M. Alotaibi, M.I. Sayyed, Ashok Kumar, Mohammed Alotiby, K.A. Mahmoud, Haifa A. Al-Yousef, N.A.M. Alsaif, Y. Al-Hadeethi, Fabrication of TeO_2-doped strontium borate glasses possessing optimum physical, structural, optical and gamma ray shielding properties, European Physical Journal Plus 136 (2021) 468.
[28] Aljawhara H. Almuqrin, M.I. Sayyed, S. Hashim, Ashok Kumar, Exploring the impact of PbO/CdO composition on the structural, optical, and gamma ray shielding properties of dense PbO–TeO_2–CdO glasses, Opt. Mater. 138 (2023) 113698.
[29] ÖzgürFıratÖzpolat ErdemŞakar, M.I. BünyaminAlım, Sayyed, Murat Kurudirek, Phy-X/PSD: development of a user-friendly online software for calculation of parameters relevant to radiation shielding and dosimetry, Radiat. Phys. Chem. 166 (2020) 108496.
[30] Sung-Hung Lan, Chin-Tung Lee, Yi-Sheng Lai, Chien-Chon Chen, Hsi-Wen Yang, The relationship between the structure and thermal properties of Bi_2O_3-ZnO-B_2O_3 glass system, Advances in Condenced Matter Physics 2321558 (2021), https://doi.org/10.1155/2021/2321558.
[31] Hanan Al-Ghamdi, Aljawhara H. Almuqrin, M.I. Sayyed, Ashok Kumar, The physical, structural and the gamma ray shielding effectiveness of the novel Li_2O-K_2O–B_2O_3–TeO_2 glasses, Results Phys. 29 (2021) 104726.
[32] S. Mohan, S. Kaur, P. Kaur, D.P. Singh, Spectroscopic investigations of Sm^{3+}-doped lead alumino-borate glasses containing zinc, lithium and barium oxides, J. Alloys Compd. 763 (2018) 486–495.
[33] M.G. Moustafa, M.Y. Hassaan, Optical and dielectric properties of transparent ZrO2TiO2–Li2B4O7 glass system, J. Alloys Compd. 710 (2017) 312–322.
[34] A.K. Hassan, L. Börjesson, L.M. Torell, The boson peak in glass formers of increasing fragility, J. Non-Cryst. Solids 172–174 (1994) 154–160.
[35] W.L. Konijnendijk, H. Verweij, Structural aspects of vitreous PbO·2B2O3 studied by Raman scattering, J. Am. Ceram. Soc. 59 (1976) 459–461.
[36] M. Farouk, Effect of Co2+ ions on the ligand field, optical, and structural properties of ZnLiB glasses, Optik 140 (2017) 186–196.
[37] A.M. Azhra, C.Y. Zahra, DSC and Raman studies of lead borate and lead silicate glasses, J. Non-Cryst. Solids 155 (1993) 45–55.
[38] N.C.A. de Sousa, M.T. de Araujo, C. Jacinto, M.V.D. Vermelho, N.O. Dantas, C. C. Santos, I. Guedes, The role of TiO2 in the B2O3–Na2O–PbO–Al2O3 glass system, J. Solid State Chem. 184 (2011) 3062–3065.
[39] N. Mary, M. Rebours, E. Castel, S. Vaishnav, W. Deng, A.M.T. Bell, F. Clegg, B. L. Allsopp, A. Scrimshire, P.A. Bingham, Enhanced thermal stability of high-bismuth borate glasses by addition of iron, J. Alloys Compd. 500 (2018) 149–157.
[40] G. Sangeetha, K.C. Sekhar, M.N. Chary, Md Shareefuddin, Influence of magnesium oxide on the physical and spectroscopic properties of manganese doped sodium tetra borate glasses, Optik 259 (2022) 168952.
[41] E.I. Kamitsos, M.A. Karakassides, G.D. Chryssikos, Vibrational spectra of magnesium-sodium-borate glasses: 2. Raman and mid-infrared investigation of the network structure, J. Phys. Chem. 91 (1987) 1073–1079.
[42] Y.B. Saddeek, K.A. Aly, KhS. Shaaban, Atif Mossad Ali, M.A. Sayed, Elastic, optical and structural features of wide range of CdO- Na2B4O7 glasses, Mater. Res. Express 5 (2018) 065204.
[43] L. Balachander, G. Ramadevudu, Md Shareefuddin, R. Sayanna, Y.C. Venudhar, IR analysis of borate glasses containing three alkali oxides, Sci. Asia 39 (2013) 278.
[44] H.A. El-Batal, F.A. Khalifa, M.A. Azooz, Gamma ray interaction, crystallization and infrared absorption spectra of some glasses and glass-ceramics from the system Li2O.B2O3.Al2O3, Indian J. Pure Appl. Phys. 39 (2001) 565–573.
[45] H.B. Pan, X.L. Zhao, X. Zhang, et al., Strontium borate glass: potential biomaterial for bone regeneration, J. R. Soc. Interface 7 (2010) 1025–1031.
[46] S. Rada, T. Ristoiu, M. Rada, I. Coroiu, V. Maties, E. Culea, Towards modeling gadolinium–lead–borate glasses, Mater. Res. Bull. 45 (2010) 69–73.
[47] K. Kotkova, H. Ticha, L. Tichy, Raman studies and optical properties of some $(PbO)_x(Bi_2O_3)_{0.2}(B_2O_3)_{0.8-x}$ glasses, J. Raman Spectrosc. 39 (2008) 1219–1226.
[48] J. Leciejewicz, Neutron-diffraction study of orthorhombic lead monoxide, Acta Crystallogr. 14 (1961) 66.
[49] Avadhesh Kumar Yadav, Prabhakar Singh, A review of structure of oxide glasses by Raman spectroscopy, RSC Adv. 5 (2015) 67583–67609.
[50] M. Ganguli, K.J. Rao, Structural role of PbO in Li2O–PbO–B2O3 glasses, J. Solid State Chem. 145 (1999) 65–76.
[51] G. Padmaja, P. Kistaiah, Infrared and Raman spectroscopic studies on alkali borate glasses: evidence of mixed alkali effect, J. Phys. Chem. A 113 (2009) 2397–2404.
[52] A.A. Kharlamov, R.M. Almeida, J. Heo, Vibrational spectra and structure of heavy metal oxide glasses, J. Non-Crys. Solid. 202 (1996) 233–240.
[53] Feng He, Zijun He, Junlin Xie, Yuhui Li, IR and Raman spectra properties of Bi_2O_3-ZnO-B_2O_3-BaO quaternary glass system, Am. J. Anal. Chem. 5 (2014) 1142–1150.
[54] Al-B.F.A. Mohammed, G. Lakshminarayana, S.O. Baki, M.K. Halimah, I.V. Kityk, M. A. Mahdi, Structural, thermal, optical and dielectric studies of Dy^{3+}: B_2O_3–ZnO–PbO– Na_2O–CaO glasses for white LEDs application, Opt. Mater. 73 (2017) 686–694.
[55] Jamelah S. Al-Otaibi, Aljawhara H. Almuqrin, M.I. Sayyed, Ashok Kumar, Multifaceted analysis of PbO–Bi2O3–ZnO–B2O3 glasses: unveiling structural, Optical, and gamma-ray shielding behaviour, J. Mater. Sci. Mater. Electron. 34 (2023) 1721, https://doi.org/10.1007/s10854-023-11166-3.
[56] M.I.Sayyed, PbO–PbF_2–B_2O_3–SiO_2 glasses: Exploring the impact of PbF_2 in modulating radiation shielding characteristics, Silicon https://doi.org/10.1007/s12633-023-02764-1.